

# Aucamp: An Underwater Camera-Based Multi-Robot Platform with Low-Cost, Distributed, and Robust Localization

Jisheng Xu

Jimmy\_xu@sjtu.edu.cn  
Shanghai Jiao Tong University  
China

Ding Lin

tysjdlin@sjtu.edu.cn  
Shanghai Jiao Tong University  
China

Pangkitt Fong

fpjgaoge@sjtu.edu.cn  
Shanghai Jiao Tong University  
China

Chongrong Fang

crfang@sjtu.edu.cn  
Shanghai Jiao Tong University  
China

Jianping He

jphe@sjtu.edu.cn  
Shanghai Jiao Tong University  
China

Xiaoming Duan

xduan@sjtu.edu.cn  
Shanghai Jiao Tong University  
China

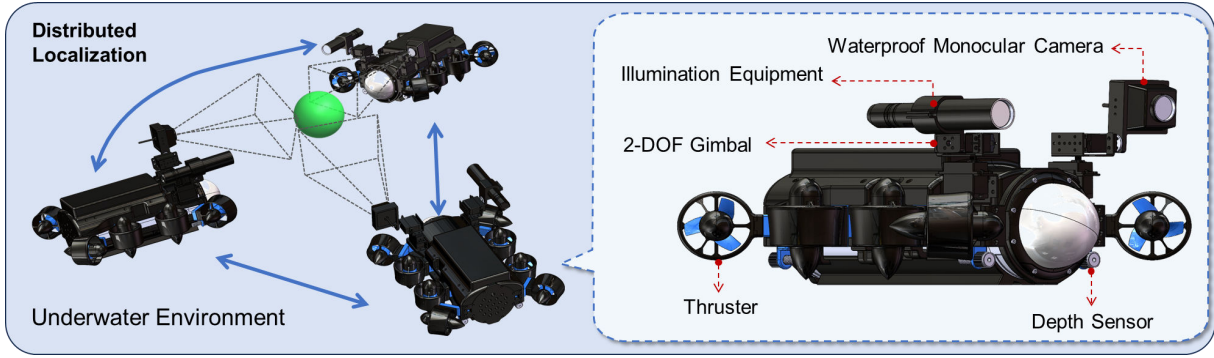


Figure 1: Aucamp is a underwater multi-robot platform that provides low-cost and robust distributed localization.

## ABSTRACT

This paper introduces an underwater multi-robot platform, named Aucamp, characterized by cost-effective monocular-camera-based sensing, distributed protocol and robust orientation control for localization. We utilize the clarity feature to measure the distance, present the monocular imaging model, and estimate the position of the target object. We achieve global positioning in our platform by designing a distributed update protocol. The distributed algorithm enables the perception process to simultaneously cover a broader range, and greatly improves the accuracy and robustness of the positioning. Moreover, the explicit dynamics model of the robot in our platform is obtained, based on which, we propose a robust orientation control framework. The control system ensures that the platform maintains a balanced posture for each robot, thereby ensuring the stability of the localization system. The platform can swiftly recover from an forced unstable state to a stable horizontal posture. Additionally, we conduct extensive experiments and application scenarios to evaluate the performance of our platform. The proposed new platform may provide support for extensive marine exploration by underwater sensor networks.

## 1 INTRODUCTION

Recent years have witnessed the rapid development of underwater robotic systems, thanks to their wide application in aquatic environment protection [5, 23], seabed resources exploration [26], ocean mapping [17], and so on. These applications highly depend on the localization capability of the underwater robotic platform.

Localization refers to the process by which the robotic system obtains the position information of a target object. For example, in marine pipeline surveillance [11], it is essential for the underwater robot to maintain a stable posture in water and perceive the position of the marine infrastructure. Similarly, the premise of well-performed underwater formation control [3] is that each robot cost-effectively locates its peers within the collective formation in a distributed way.

In this paper, we endeavor to design a cost-effective and practical underwater multi-robot platform equipped with a distributed and robust localization framework. To meet the needs of underwater localization in various tasks, a multi-robot platform should obtain the following three capabilities:

**1) Cost-effective sensing.** A multi-robot platform is capable of conducting large-scale perceptual tasks concurrently. However, equipping each robot with precise and costly sensors would lead to an excessively high overall cost for the

platform. Therefore, each robot should achieve sufficiently effective perception with relatively low-cost sensors.

**2) Distributed update protocol.** In aquatic environments characterized by communication impediments, a centralized protocol can lead to excessive communication pressure on the central node. Moreover, due to the complexity of the underwater environment, the loss of connection with the central node could result in the collapse of the entire platform. A distributed iterative strategy is necessary for ensuring flexibility and robustness of the system.

**3) Robust orientation control.** For a robot to perceive and locate a target object, it is imperative to first ensure the stability of its own orientation. Since the underwater environment replete with currents, turbulence and marine lives, an underwater robotic system needs precise dynamic analysis and the establishment of an appropriate orientation control strategy to counteract potential external disturbances.

However, to the best of our knowledge, no existing underwater robotic platform satisfy all these three requirements. In this paper, we present An Underwater Camera-Based Multi-Robot Platform named **Aucamp**, equipped with low-cost, distributed, and robust localization. Aucamp is the first multi-robot platform systematically designed for distributed localization, by addressing low-cost perception (monocular-camera-based), designing a distributed framework, and providing robust orientation control mechanisms.

## 1.1 Related Work

Underwater robotic platforms are fundamentally related to the development of underwater sensors. According the localization sensors they carry, existing platforms can be categorized into four types: Acoustic sensor-based platforms, electromagnetic wave sensor-based platforms, inertial sensor-based platforms, and optical sensor-based platforms.

**1) Acoustic sensor-based platforms:** Acoustic sensors like sonars are commonly used in multiple underwater robotic platforms [2, 4, 8, 20]. For example, AQUA [6] use Synthetic Aperture Sonar (SAS) for achieving centimeter-resolution for detailed seabed mapping, and Multibeam Forward-Looking Sonars (FLSs) for obstacle avoidance and navigation enhancement. These sensors can procure the positions of objects and obstacles on the seabed and accomplish localization tasks. However, acoustic sensors work by emitting sound waves and measuring the time it takes for the waves to bounce back from objects. Constrained by the speed of sound, their range measurement has a high latency. Besides, high-precision multi-beam acoustic sensors are often prohibitively expensive, usually costing several hundred thousand dollars, which is unacceptable for multi-robot platforms.

**2) Electromagnetic wave sensor-based platforms:** Sensors based on electromagnetic waves, such as the Global

Positioning System (GPS), Global Navigation Satellite System (GNSS), and Ultra-Wideband (UWB), are specifically designed for localization. Numerous robotic platforms integrate these sensors to achieve self-localization and navigation within their operational environments [1, 15, 24, 25]. However, due to the absorption of electromagnetic waves by water, sensors based on electromagnetic waves are attenuated when more than 10cm away from the water surface, which is not suitable for underwater environment.

**3) Inertial sensor-based platforms:** Inertial sensors, i.e., Inertial Measurement Units (IMUs), consist of accelerometers and gyroscopes that measure linear accelerations and angular velocities, respectively. By integrating these measurements over time, the velocity and orientation of an object can be determined. For instance, LoCO [7] present a low-cost underwater unmanned vehicle that use IMU to obtain the localization of the robot itself. Similarly, bionic cross-media robots like [21] also utilize IMU to stabilize the orientation of the robot. However, owing to the inherent nature of IMUs to perform integration, platforms that rely on IMUs have significant cumulative errors. Additionally, IMUs can only obtain the positioning of the robot itself and are unable to locate external objects.

**4) Optical sensor-based platforms:** Optical sensors can be further categorized into active optical sensors and passive sensors. Active sensors, which requires the emission of light, are broadly used in existing platforms, including LiDAR [31], depth cameras[27, 28], and other custom sensors [16]. These sensors are ineffective underwater due to the absorption effect of water on light. Common passive optical sensors include binocular stereo vision cameras and ordinary cameras. Some studies have proposed methods for range and locate objects underwater based on binocular cameras [9, 32]. However, due to the need for feature matching, the application of binocular cameras is limited in underwater environments where feature points are sparse. Likewise, the principle of triangulation requires that the two cameras of the binocular system be as far apart as possible, which is contrary to the compactness required for sensors on underwater robots.

The aforementioned analysis of related underwater robotic platforms is summarized in Table 1. Existing work are inadequate to address the problem of low-cost robust localization in a distributed way. In this paper, we utilize monocular cameras to design a multi-robot platform and provide cost-effective, distributed, and robust localization. Compared with other robotic platforms, the monocular camera we use is the cheapest and the most compact sensor that can be used for underwater localization.

**Table 1: Existing localization-related sensors that underwater robotic platforms carry**

Sensor type	Representative platforms	Accuracy	Cost	Underwater characteristic
Acoustic sensors	[2, 4, 6, 8, 20]	High (at long distance)	Very high	High latency
Electromagnetic wave sensors	[1, 15, 24, 25]	Medium (on land)	Medium	Invalid underwater
Inertial sensors	[7, 21]	Low (with cumulative error)	Low	Limited to robot localization
Active optical sensors	[16, 27, 28, 31]	High (on land)	High	Invalid underwater
Binocular cameras	[9, 32]	Medium	Low	Insufficiently compact structure
<b>Monocular cameras</b>	<b>Aucamp (our work)</b>	<b>Medium</b>	<b>Low</b>	<b>Lack depth information</b>

## 1.2 Challenges

As mentioned in previous subsection, considering the constraints of cost and the underwater environment, we choose monocular cameras for localization. However, a single monocular camera itself cannot achieve underwater localization. To achieve underwater monocular-camera-based localization, it is necessary to address the following four challenges:

**1) Lack of visual ranging capabilities.** Cameras inherently provide only two-dimensional spatial information. Monocular cameras are unable to measure distances accurately because they cannot perceive depth from a single image without additional information.

**2) Limited field of view.** For localization purposes, a single monocular camera provides only a relatively limited field of view. In the intricate underwater environment, the absence of light sources and the presence of various underwater obstacles can further diminish the actual visual range.

**3) Poor underwater imaging quality.** The visual quality of images captured underwater is often compromised due to factors such as water turbidity and light absorption. The scattering of light by suspended particles in the water can result in image blurriness and loss of feature. The absorption of light by water at different wavelengths can lead to severe color bias in images. Consequently, many image processing algorithms that perform well on land are ineffective in underwater environments.

**4) Complex environment.** The underwater fluid dynamics environment is characterized by a high degree of complexity, which poses significant challenges for the control of underwater robots. Because of various currents and vortices, the attitude control of robots is highly vulnerable to interference from the external forces.

In this paper, we undertake many designs to address the aforementioned challenges. For visual ranging, we establish the intrinsic relationship among the focusing range and the object distance, thus achieving depth estimation of underwater monocular cameras. A distributed update protocol is designed for our multi-robot platform to perceive a broader area simultaneously. When one robot in our platform detects a target object, it can inform other robots to take multi-angle shots and localize the target object more accurately.

To improve the imaging quality, we employ a lightweight underwater image enhancement algorithm to enhance the underwater images in real-time. Moreover, to support these designs, a robust orientation control framework is presented to ensure that the robot maintains a stable posture during sensing and localization.

## 1.3 Contributions and Organization

In this paper, we present an underwater multi-robot platform for cost-effective distributed localization, named Aucamp. Unlike existing solutions, the underwater multi-robot platform designed in this paper is the first to systematically employ low-cost monocular cameras for underwater localization. Outfitted with a distributed iteration framework and a resilient control system, the platform is capable of delivering stable and robust localization within a distributed multi-sensor network. This makes it well-suited for a variety of intricate underwater missions, including the tracking of aquatic organisms and the 3D reconstruction of underwater scenes. Our main contributions are summarized as follows:

- We propose an underwater multi-robot platform based on low-cost monocular cameras. To the best of our knowledge, it is the first underwater robotic platform that systematically attains cost-effective, distributed, and robust localization.
- To address the challenge of localization with underwater monocular cameras, we integrate clarity features (Tenengrad function) into a monocular camera, supplemented by underwater image enhancement algorithm and underwater camera modeling, achieving low-cost monocular underwater positioning.
- A distributed update mechanism and a robust control framework are obtained, enabling the proposed underwater multi-robot platform to accomplish complex tasks such as tracking marine life and 3D reconstruction of underwater scenes. Experimental validations and application instances are also conducted.

The rest of this paper is structured as follows: Section 2 provides an overview of our proposed underwater multi-robot platform, including an introduction to the components and the platform workflow. Section 3 focuses on our design on monocular-camera-based underwater perception. Sections 4

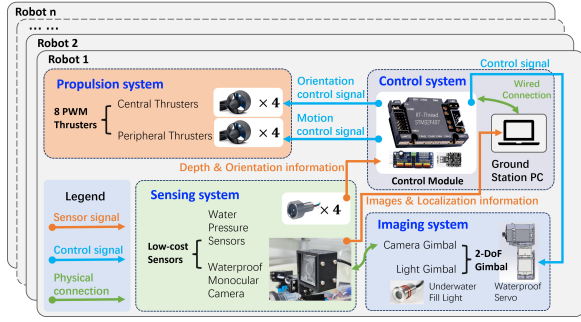


Figure 2: Architecture of Aucamp.

and 5 respectively detail the distributed localization protocol and orientation control system of our platform. Section 6 presents experimental evaluation results, coupled with application scenarios like marine life tracking and underwater distributed 3D reconstruction. Finally, Section 7 concludes the paper and discusses potential future research directions.

## 2 PLATFORM COMPONENTS AND IMPLEMENTATION

As illustrated in Figure 2, Aucamp is composed of several identical robots, each equipped with control system, propulsion system, sensing system, and imaging system. We will provide the details of the design and specific implementation of each system, followed by a demonstration of the relationships of these systems using the platform workflow.

**1) Control system.** Each robot in the platform adopts a supervisory and subordinate machine structure, where the supervisory machine is a ground station computer that serves as a medium for communication among robots within the platform; the subordinate machine is the control module of each robot, tasked with aggregating sensor data, executing control algorithms, and dispatching directives to the actuators, ultimately achieving collaborative positioning, planning, and control of the platform.

To implement such a structure, each robot is endowed with a control module, complemented by corresponding interface expansion, power supply, and information transmission equipment. The control module is based on the STM32F407 micro-controller, housed within a sealed, waterproof compartment of each robot. All the control modules of every robots are connected to the base station computer via cables. Camera image data, which is too memory-intensive, is processed by the ground computer to derive object positioning data, which is then relayed to the low-level control module. All other sensory data is managed by the control module itself. The control signals for the actuators are also generated and dispatched by the control module.

**2) Propulsion system.** Propulsion system is designed for the orientation control and the motion control of each robotic

body. The propulsion system consists of eight thrusters, four of which are fixed in the central part of the robot, and the other four are located at the periphery. The central thrusters are responsible for controlling the orientation and the hovering depth of the robot, while the peripheral thrusters are responsible for controlling the forward, backward, lateral, and rotational movements.

In implementation, all thrusters are regulated by the control system through PWM (Pulse Width Modulation). The thrusters with clockwise rotation and those with counter-clockwise rotation are arranged alternately, ensuring that the reaction torque generated by the rotation of the thrusters does not affect the movement of the robot. Each thruster has a distinct initial PWM value. When the PWM input to a thruster exceeds its initial value, it rotates in the forward direction; when it is below the initial value, it rotates in the reverse direction. We control the speed and direction of each thruster by adjusting the delta PWM (the change in PWM value from the initial setting).

**3) Sensing system.** The sensing system of each robot is equipped with a monocular camera to support low-cost distributed localization, and four water pressure sensors for robust orientation control. Inspired by [13], pressure sensors can measure the fluid pressure exerted at different locations on the robot, which can be utilized to sense water depth and achieve better posture control. These four pressure sensors are able to obtain orientation data of the robot on two angular axes through pairwise differential measurements.

In the specific implementation, each monocular camera is an ordinary camera with a price of less than \$50, capable of manually focusing through control signals from computer (similar to the camera module of a smartphone). Each monocular camera is sealed in an individual transparent acrylic waterproof housing, fixed on a two-degree-of-freedom camera gimbal, and its motion is driven by the movement of the gimbal. The pressure sensing data is transferred to control module to process, and used to control the central thrusters of the propulsion system.

**4) Imaging system.** Each underwater robot in our platform mounts the camera and illumination light on two 2-degree-of-freedom (2-DoF) gimbal and incorporates a waterproof design. When dealing with complex underwater tasks such as tracking rapidly moving underwater objects, this design allows the imaging system to be decoupled from the motion of the underwater robot and controlled independently, thereby providing the illumination and imaging system with greater flexibility. In the implementation, each gimbal is composed of two waterproof servos arranged vertically and fixed in relation to each other. The servos are control by the control module through PWM.

**Platform workflow:** Here is a brief overview of how the various systems coordinate with each other. For orientation



control, the sensing system acquires depth information from different positions of the robot and transmits it to the control system, which calculates the orientation of the robot. Based on the orientation information, the control system determines the required rotation speed for the central thrusters and sends it via PWM signals to each central thruster in the propulsion system.

For object positioning, the cameras of the sensing system of every robots obtain positional data of the target object. Subsequently, the control system calculates the necessary angular displacement for the gimbal in imaging system, actuating the gimbal to pivot with PWM and align the camera with the target object. Should the rotation of camera gimbal prove inadequate, the control system will determine the necessary rotational velocity for the peripheral thrusters of the propulsion system, facilitating the movement of the entire robot to align the camera with the target object.

Each robot utilizes its camera-based perception system to ascertain the position of target object. Once a robot within the platform identifies the target object, it estimates the location of the object through its monocular camera localization system and communicates this information with the other robots, initiating distributed location estimation for the object. The proposed distributed update protocol ensures consistency in the location estimation of the object by each robot, and ultimately achieves distributed localization.

Over the next three sections, we will provide the details of our proposed underwater multi-robot platform, including the approaches to realizing camera-based perception, the cooperative distributed localization algorithm, and the mechanisms for ensuring stable orientation control.

### 3 MONOCULAR-CAMERA-BASED UNDERWATER PERCEPTION

In the platform designed in this paper, each robot is equipped with a cost-effective monocular camera. Essentially, the digital camera provides a two-dimensional matrix across the RGB channels, which indicates the two-dimensional spatial information of the imaged object. However, in various applications, three-dimensional localization of the object is often required. This necessitates the estimation of depth, i.e., the orthogonal distance between the camera and the underwater object of interest. Therefore, this section will present a method for depth estimation using only a monocular camera.

#### 3.1 Monocular Depth Estimation

This subsection will specifically elaborate on how to use the regional clarity differences obtained by a monocular camera to derive depth information from images.

**3.1.1 Underwater image enhancement.** The original images captured by underwater cameras often exhibit poor quality

due to the severe distortion caused by the refraction and absorption of light. To improve the underwater imaging performance of monocular cameras, we firstly introduce LU2Net [34], a lightweight underwater image enhancement model, into our platform. Figure 3a and Figure 3b illustrate the original image and enhanced image by LU2Net, respectively.

It is apparent that the image enhancement algorithm we utilize has effectively mitigated the issues of color distortion and blurriness in underwater images, thus supporting subsequent depth estimation procedures. Notably, LU2Net operates in real time (up to 100 frames per second), thereby allowing for non-time-consuming integration onto the platform without any negative effect on our perception.



(a) Original image

(b) Enhanced image

**Figure 3: Underwater image enhancement result.**

**3.1.2 Clarity feature.** As summarized in Table 1, most camera-based localization solutions cannot be directly transferred to underwater environments. This is due to their reliance on additional electromagnetic wave (light) emission and reception devices for positioning, which are prone to malfunction underwater. Existing researches have extensively study the solutions on land. The key reason why they is that they all rely to some extent on absolute features in the image, rather than relative features. Absolute features are vulnerable to poor lighting condition underwater. To facilitate localization using only a monocular camera, it is essential to extract depth information from the images generated by the camera itself for the purpose of distance measurement.

Our insight reveals that the differences in clarity across various regions in the image represent a relative feature that can be used for distance measurement, and relative features are independent of whether the camera is on land or underwater. This suggests the potential to utilize clarity for underwater monocular depth estimation.

As illustrated in Figure 4a, there are both clear areas and blurry areas in a image captured by a monocular camera. Apparently, the clear area is closer to the camera than the blurry one, which indicates that clarity feature contains depth information. To apply this idea, we employ the Modified Tenengrad function  $T$  [30], an indicator of clarity. For a given region  $R$ , a higher value of this operator  $T(R)$  indicates greater clarity in the imaging of that area.

For a specific region  $R$  within Figure 4a, one can obtain Figure 4b by changing the focus distance from the nearest to

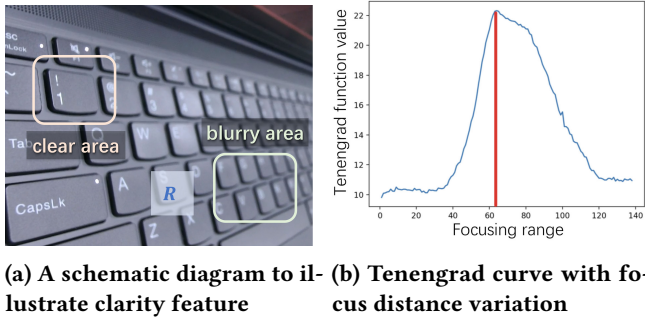


Figure 4: Illustration of Tenengrad clarity feature.

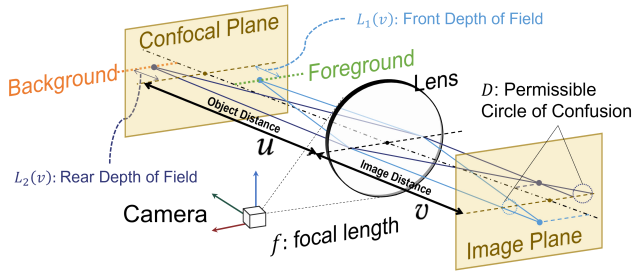


Figure 5: The monocular depth estimation system.

the farthest and calculating the Tenengrad function value for each focus distance. It can be observed that the  $T$  is a single-peaked function with respect to focus distance. For a region  $R$ , there exists a unique optimal focus distance. We can utilize this characteristic for monocular distance measurement.

**3.1.3 Monocular distance measurement.** As shown in Figure 5, the monocular camera is simplified as a single-lens system. Based on fundamental optics [10], we have:

$$\frac{1}{f} = \frac{1}{v} + \frac{1}{u}, \quad (1)$$

where  $f$  is the focal length of the camera,  $v$  represents the image distance (the distance from the lens to the image plane), and  $u$  signifies the object distance (the distance from the object to the lens). If  $v > f$ , (1) is equivalent to

$$u = \frac{fv}{v - f} \triangleq u(v), \quad (2)$$

which suggests that, given the known focal length  $f$  of the camera's equivalent lens, by ascertaining the image distance  $v$ , one can deduce the object distance  $u$ , that is, the depth information we required. With a monocular camera, this facilitates the process of three-dimensional object localization.

As mentioned before,  $T(R)$  indicates the clarity. When  $T(R)$  is at its peak, it implies that the object distance  $u_R$  of the objects in that region  $R$  conforms to (2). In this paper, we employ a monocular camera with manual-focus capabilities, which can change the image distance  $v$  by adjusting the

position  $\rho$  of the built-in voice coil motor. Therefore,

$$v = g(\rho), \quad \rho^* \triangleq \arg \max_{\rho} T(R), \quad u_R = \frac{fg(\rho^*)}{g(\rho^*) - f},$$

where  $\rho^*$  is the best position of voice coil motor within the camera. Based on our extensive experiments, we claim that the following empirical formula accurately describes the relationship between the variables  $u_R$  and  $\rho^*$ :

$$g(\rho) = \kappa\rho, \quad h(\rho^*) \triangleq \frac{f\kappa\rho^*}{\kappa\rho^* - f} + c, \quad u_R = h(\rho^*) + L(v), \quad (3)$$

where  $\kappa$  and  $c$  are constants determined by the physical characteristic of the monocular camera,  $L(v)$  is the error (will be discussed in the next subsection), and the unknown  $\kappa$  and  $c$  in function  $h$  can be fit through experiments. Equation (3) implies that the input-output relationship of the focusing module in the camera to be linear. Furthermore, given the inaccuracy in precisely determining the central position of the equivalent lens of a monocular camera, a constant  $c$  is incorporated into (3) to represent the positional offset.

### 3.2 Localization with Monocular Camera

In the previous subsection, we present the approach obtain the object distance  $u_R$ , i.e., the vertical distance between the monocular camera and object. In this subsection, we use camera imaging model to obtain the object localization  $[x_{\text{obj}}, y_{\text{obj}}, z_{\text{obj}}]^T$ , and further analyze the theoretical error of this monocular localization.

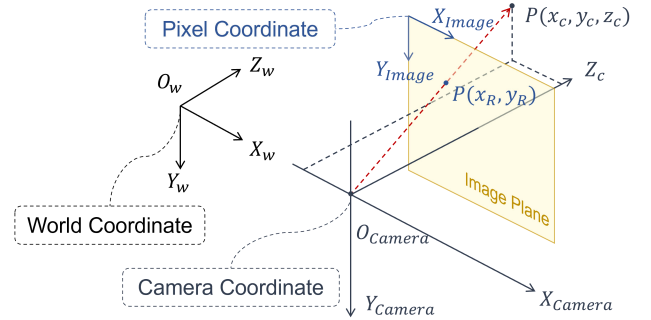


Figure 6: The monocular camera imaging model.

**3.2.1 Camera imaging model.** As shown in Figure 6, a calibrated camera can be regarded as a pinhole camera that satisfies the monocular camera imaging model, which can be described by:

$$[x_R, y_R, 1]^T = \frac{1}{z_c} \Theta [x_c, y_c, z_c]^T,$$

where  $\Theta$  represents the intrinsic matrix of the camera,  $[x_R, y_R]^T$  is the pixel coordinates of the object, and  $[x_c, y_c, z_c]^T$  corresponds to the position of the object in camera coordinate system. The intrinsic matrix  $\Theta$  is invertible and can be determined using various calibration methods [22]. Note that

$z_c$  is the vertical distance from the object to the camera, i.e.,  $z_c = u_R$ . Therefore, given the pixel coordinates  $[x_R, y_R]^T$  and the depth  $u_R$  the target, the object coordinates in the world coordinate system are:

$$\hat{x} = \begin{bmatrix} x_{\text{obj}} \\ y_{\text{obj}} \\ z_{\text{obj}} \end{bmatrix} = R_c^O \begin{bmatrix} x_c \\ y_c \\ z_c \end{bmatrix} + p_c^O = u_R R_c^O \Theta^{-1} \begin{bmatrix} x_R \\ y_R \\ 1 \end{bmatrix} + p_c^O, \quad (4)$$

where  $R_c^O$  and  $p_c^O$  represent the rotation matrix and the translation matrix from camera coordinate system  $O_c$  to the world coordinate system  $O_w$ . The hat of variable  $\hat{x}$  indicates that this value is obtained by the monocular-camera-based localization presented in this section. Thus, (4) provides a method for localization using a single monocular camera.

**3.2.2 Localization error analysis.** The sources of error in the aforementioned localization model are twofold: systematic errors in the depth estimation process, and the impact of the underwater environment on the imaging model.

Our monocular depth estimation approach suggests that the depth of a target object can be ascertained by identifying the focus range in a monocular camera, at the point when the region of that object in the image achieves maximum clarity. However, it is based on the implicit assumption that a single image distance  $v$  corresponds to a single object distance  $u$ , meaning that when the image distance  $v$  is constant, only the points on a plane at a specific distance  $u(v)$  are in focus in the photograph. This assumption is idealized and does not take into account the issue of *depth of field*.

As illustrated in Figure 5, due to the physical dimensions  $D$  of the smallest unit of the camera's photosensitive element (often termed CMOS), all objects within the range  $[u(v) - L_1(v), u(v) + L_2(v)]$  appear sharp. The distance measured by our method therefore has a certain degree of error, the magnitude of which is the depth of field  $L(v) \triangleq L_1(v) + L_2(v)$ . According to [10], the measurement error of our method, i.e., the depth of field  $L(v)$  satisfy  $L(v) = \frac{f^2 u}{f^2 - \Gamma D(u - f)} - \frac{f^2 u}{f^2 + \Gamma D(u - f)}$ , where  $\Gamma$  is the aperture value of the monocular camera.

Besides, due to the necessity for underwater cameras to be waterproof, an additional waterproof housing is often required compared to cameras used on land. The housing and the refraction of light by water can affect the monocular-camera-based localization model. According to [12], the impact of the underwater environment on the camera is primarily manifested in the alteration of the intrinsic matrix  $\Theta$  and the camera's equivalent focal length  $f$ . In our localization approach, the intrinsic matrix  $\Theta$  can be corrected by recalibration underwater. The camera's equivalent focal length  $f$ , which is a coefficient in the ranging function  $h$ , can also be ascertained through underwater calibration. Therefore,

the underwater environment has negligible impact on our localization method.

## 4 DISTRIBUTED UPDATE PROTOCOL FOR GLOBAL LOCALIZATION

For underwater multi-robot platforms, obtaining global localization is challenging. Not every robot within the platform has access to the target object's field of view in its initial state. Fortunately, as described in the previous section, each robot has been endowed with the capability for monocular object localization. Consequently, provided that at least one robot within the platform has the target object in its field of view, coupled with the distributed iterative strategy presented in this section, the localization information of the target object will propagate throughout the entire multi-robot platform. Therefore, through interaction with neighboring robots, each robot in the platform can contribute to a more precise distributed positioning of underwater objects.

This section will first introduce the basic network topology settings, then present the update protocol, and finally analyze the global localization process of the platform.

### 4.1 Network Topology and Update Protocol

Consider a underwater platform that consists of  $N$  robots. The topology of the multi-robot platform can be formulated as an connected undirected graph  $G = (V, E)$ , where  $V = \{1, 2, \dots, N\}$  and  $E \subset V \times V$  denote the nodes and the edges of  $G$ , respectively. Each node  $i \in V$  represents a robot. Each edge  $e_{ij} = (i, j) \in E$  suggest that robot  $i$  and robot  $j$  can communicate with each other in the platform. Define  $N_i \triangleq \{j \in V | (i, j) \in E\}$  as the neighborhood set of robot  $i$ . The degree of robot  $i$  is defined by  $d_i \triangleq |N_i|$ .

In each iteration  $t$ , based on the method from the previous section, each robot can obtain the position of the target object through monocular depth estimation. This positional information, noted as  $\hat{x}_i^t$ , will serve as the a prior estimation of the target object's location for each robot. As shown in Figure 7, each robot send its  $x_i^t$  to all its neighbors, gather information from them, and derive a new a posterior estimation  $x_i^{t+1}$  based on its prior estimation  $\hat{x}_i^t$  and neighborhood information, thereby achieving a more accurate distributed localization of the target object.

At every iteration  $t$ , each robot  $i$  in the platform maintains its local state variable  $x_i^t$ , i.e., the estimation for the location of target object. Note that the object of interest may not be within the visual range of every robot, and due to the movement of the robots and the variability of the underwater environment, there is a possibility that the robots may be obstructed or lose track of the target object. Therefore, we introduce the *valid robot set*  $S^t \subset V$  for every iteration  $t$ . All the robots within  $S^t$  have the view of the target object.

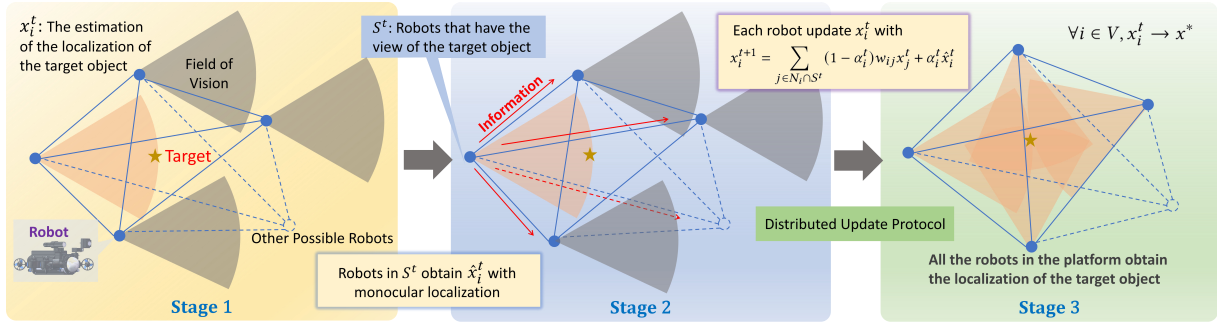


Figure 7: Distributed update protocol.

For robots in the set  $V \setminus S^t$ , since the prior estimation  $\hat{x}_i^t$  is meaningless, they determine their local estimation only based on all neighbors in the valid robot set. Our update protocol follows

$$\forall i \in V, t \geq 0, \quad x_i^{t+1} = \sum_{j \in N_i \cap S^t} (1 - \alpha_i^t) w_{ij} x_j^t + \alpha_i^t \hat{x}_i^t, \quad (5)$$

where  $w_{ij}$  the weight,  $\forall j \notin N_i, w_{ij} = 0$ , and the step size  $\alpha_i^t$  satisfy  $\forall i \notin S^t, \alpha_i^t = 0$ . If  $N_i \cap S^t \neq \emptyset, \forall i \in V, \alpha_i^t \leq O(\frac{1}{t})$ . If  $N_i \cap S^t = \emptyset, \alpha_i^t = 1$ . For  $t = 0$ , we have

$$\forall i \in S^0, x_i^0 := \hat{x}_i^0.$$

Our protocol is designed based on the *Average Consensus Algorithm* from the field of distributed optimization [19] and the  $\epsilon$ -greedy *Algorithm* from Reinforcement Learning [29]. In (5), the term  $w_{ij} x_j^t$  is inspired by Average Consensus Algorithm, which is presented for reaching a common value among a group of agents in a network through local communication and information exchange. The introduction of  $\alpha$  borrows the concept from the  $\epsilon$ -greedy Algorithm, allowing each robot to consider both its own observations based on the sensory system and those of its neighbors. Besides, by making  $\alpha_i^t$  gradually approach 0, the robot  $i$  gradually disregard its own local observations, thereby achieving globally consistent distributed localization. Our distributed update protocol design is summarized in Algorithm 1.

## 4.2 Global Localization

Through the aforementioned design, the update protocol (5) allows robots that initially lack the view of the target object to calculate an approximate location through information from their neighbors. Subsequently, they adjust the orientation of their cameras to ultimately obtain a visual field of the target object. Once a robot acquires the target in its field of view, it joins the set  $S^t$ , which gradually expands until  $S^t$  coincides with set  $V$ , ensuring that all robots have a visual field of the target object. Concurrently, the protocol integrates observation data from multiple steps and multiple robots, reducing the impact of observational noise on positioning.

---

### Algorithm 1: Distributed Localization

---

```

1 Initialize  $S^0$ ;
2 for agent  $i \in S^0$  do
3    $x_i^0 := \hat{x}_i^0$ ;
4 end
5 for agent  $i \in \mathcal{V}$  do
6   for  $t = 0, 1, 2, \dots, T$  do
7     Try to obtain  $\hat{x}_i^t$ . Update  $S^t, \alpha_i^t$ ;
8     if agent  $i \in S^t$  then Send  $x_i^t$  to neighbors
9        $j \in N_i$ ;
10    Gather  $x_j^t$  from all the neighbors  $j \in N_i \cap S^t$ ;
11    Calculate  $x_i^{t+1}$  with (5);
12  end
13 end
Output:  $\{x_i^T\}$ .

```

---

Noted that the variable  $\hat{x}_i^t$  is the measured value of the true position of the target object, we have

$$\forall i \in V, t \geq 0, \exists \delta, \quad \text{s.t.} \quad \hat{x}_i^t = x^* + \delta, \quad (6)$$

where  $x^*$  is the true position of the target object, and  $\delta$  represents the measurement noise. Usually, this noise is a zero-mean Gaussian distribution related to the performance of the sensors, i.e.,

$$\delta \sim \mathcal{N}(0, \sigma^2), \quad (7)$$

where the variance  $\sigma^2$  reflects the error in the measurement. Suppose (6) and (7) hold, according to [19], it is easy to prove that when the target object is static in position  $x^*$ , as  $t \rightarrow \infty$ , we have

$$\forall i \in V, x_i^t \rightarrow x^*.$$

This implies that, as long as the target object is initially within the field of view of any robot within the platform, over time, all robots will orient their cameras towards the object. Moreover, they all will be able to obtain the global localization of the target object.



## 5 ROBUST ORIENTATION CONTROL

The preceding sections elaborate the approach to perform distributed localization based on monocular vision. However, the foundation of this method lies in the ability to effectively control the orientation of the robot itself. Otherwise, in the complex underwater environment, if balance cannot be maintained, the camera will not be able to stably capture clear images, the localization algorithms will become ineffective.

In this section, a comprehensive dynamic analysis of our robotic systems is presented, coupled with the formulation of a well-conceived control system. This ensures that the localization is executed on a platform characterized by a stable and controlled posture.

### 5.1 Dynamics Model

In this subsection, we focus on analyzing how to control the four central thrusters to achieve orientation control of the robot. Given that the robot is capable of stable hovering, the peripheral four thrusters can influence the movements of the robot within the horizontal plane. This aspect, while straightforward, is not discussed due to space constraints.

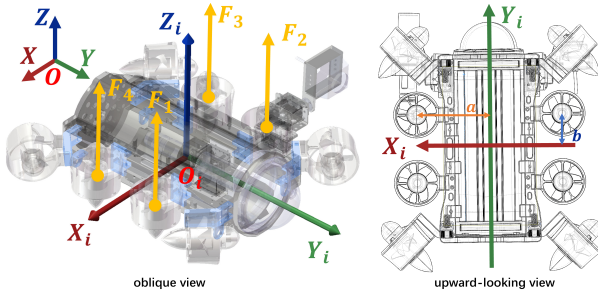


**Figure 8: Illustration of the coordinate system.**

As illustrated in Figure 8, the global coordinate system is denoted as  $O(X, Y, Z)$ , with each robot  $i$  having its own body coordinate system  $O_i(X_i, Y_i, Z_i)$ . The origin  $O_i$  is located at the central position of each robot  $i$ . Four pressure sensors and the four central thrusters are symmetrically arranged around the origin. The thrusters are positioned at distances  $a$  and  $b$  from the respective axes. Define the position vector, attitude vector, Euler angle rate vector, of the robot respectively by

$$\eta = [x, y, z], \xi = [\phi, \theta, \psi], \omega = [\dot{\phi}, \dot{\theta}, \dot{\psi}].$$

For simplicity, the subscript  $i$  indicating different robots are not included. Unless specifically indicated, all dynamic variables in this subsection are set for a single robot  $i$ . Since the platform employs homogenous robots, the dynamic analysis of one robot is applicable to all. According to Newton's second law of motion, we have:

$$m \frac{d^2 \eta}{dt^2} = F_1 + F_2 + F_3 + F_4 - [0, 0, mg]^T - F_f,$$

where  $\{F_1, F_2, F_3, F_4\}$  represent the thrust from four thrusters,  $m$  is the mass of the object,  $g$  is the acceleration of gravity, and  $F_f$  is the resistance exerted on the robot by the water body. According to fluid mechanism [14], we have

$$F_f = [k_x \dot{x}^2, k_y \dot{y}^2, k_z \dot{z}^2],$$

where  $\{k_x \dot{x}^2, k_y \dot{y}^2, k_z \dot{z}^2\}$  represent the coefficients of fluid resistance in the three axis of  $O_i$ . Define  $v_j$  as the rotational speed of the thruster  $j$ , then  $F_j = R_i^O [0, 0, K]^T v_j^2$  ( $j \in \{1, 2, 3, 4\}$ ), where  $K$  is a coefficient related to the characteristics of the thruster,  $R_i^O$  is the rotation matrix from  $O_i$  to  $O$ .

$$\begin{cases} m\ddot{x} + k_x \dot{x}^2 = K \sum_j v_j^2 (\cos \phi \sin \theta \cos \psi + \sin \phi \sin \psi), \\ m\ddot{y} + k_y \dot{y}^2 = K \sum_j v_j^2 (\cos \phi \sin \theta \sin \psi - \sin \phi \cos \psi), \\ m\ddot{z} + k_z \dot{z}^2 = K \sum_j v_j^2 \cos \phi \cos \theta - mg. \end{cases} \quad (8)$$

In the vicinity of the steady state, the torque effect of the fluid on the robot is negligible. Besides, since the actual propellers are installed in an alternating positive and negative rotation pattern, the effect of the blade rotation of the thrusters is also neglected. By Euler's theorem, the equation of rotation around the center of mass is  $M = I\dot{\omega} + \omega \times I\omega$ , where

$$I = \begin{bmatrix} I_x & 0 & 0 \\ 0 & I_y & 0 \\ 0 & 0 & I_z \end{bmatrix}, M = \begin{bmatrix} (v_1^2 + v_2^2 - v_3^2 - v_4^2)b \\ (-v_1^2 + v_2^2 + v_3^2 - v_4^2)a \\ 0 \end{bmatrix},$$

thus,

$$\begin{cases} I_x \ddot{\phi} + (I_z - I_y) \dot{\theta} \dot{\psi} = (v_1^2 + v_2^2 - v_3^2 - v_4^2)b, \\ I_y \ddot{\theta} + (I_x - I_z) \dot{\phi} \dot{\psi} = (-v_1^2 + v_2^2 + v_3^2 - v_4^2)a, \\ I_z \ddot{\psi} + (I_y - I_x) \dot{\phi} \dot{\theta} = 0. \end{cases} \quad (9)$$

The equation (8) and (9) demonstrate the dynamics model of a single robot. In the following section, we will discuss how to utilize this dynamics model for the control system design.

### 5.2 Orientation Control

In this subsection, we focus on designing a control system to keep a robot  $i$  hovering in water at a fixed depth  $z^*$ , while ensuring the main plane  $O_i X_i Y_i$  remains horizontal. Therefore, we are only concerned with the depth and orientation of the robot, i.e.,  $s \triangleq [z, \phi, \theta, \psi]^T$ . Besides, only the rotational speeds of the four thrusters in the center are controllable, denoted as  $v \triangleq [v_1, v_2, v_3, v_4]^T$ . According to the dynamics model (8)(9), it is noted that the variable  $s$  is only related to  $\sum_j v_j^2$ ,  $(v_1^2 + v_2^2 - v_3^2 - v_4^2)$  and  $(-v_1^2 + v_2^2 + v_3^2 - v_4^2)$ . Thus, define



control input  $U$  with

$$\Theta \triangleq \begin{bmatrix} 1 & 1 & 1 & 1 \\ 1 & 1 & -1 & -1 \\ -1 & 1 & 1 & -1 \end{bmatrix}, U \triangleq \Theta v v^T. \quad (10)$$

As for the sensory data, each robot in our platform is equipped with four pressure sensors, each mounted at the four corners of the robot. Pressure sensors are capable of measuring the water pressure at specific locations and obtain the water depth, which is widely used in underwater robots.

The use of multiple pressure sensors can enable more capabilities than simply measuring the depth. Inspired by the multi-pressure-sensor applications in [13], this paper also utilizes multiple pressure sensors to explore how to derive the attitude information from the pressure sensor data, thereby achieving robot orientation control. Specifically, using multiple pressure sensors as sensors and the speed of the central thrusters as the control quantity, we can model the control system and propose a robust orientation control scheme based on pressure sensors.

The pressure sensors around the robot can measure the depth at their respective positions. Denote the four output values of the pressure sensors as  $\zeta = [\zeta_1, \zeta_2, \zeta_3, \zeta_4]^T$ . Similar to (10), define  $\mu = \Theta \zeta$ . The goal is to make  $\mu$  equals to  $[4z^*, 0, 0]^T$ . Define  $e \triangleq \mu - [4z^*, 0, 0]^T$  and utilize the PI controller, we have  $U = K_p e + K_i \int e dt$ . Besides, when the robot is stationary at the target position, gravity is balanced by the thrust force of the four thrusters. Thus,

$$K \sum_j v_j^2 = mg. \quad (11)$$

Equation (10) and (11) constitute a linear system encompassing four unknown variables, which can be solved for  $[v_1^2, v_2^2, v_3^2, v_4^2]$ . Ultimately, the necessary rotational speeds of the central thrusters are obtained, thereby achieving robust orientation control of the underwater robot platform.

## 6 EVALUATION

In this section, we present extensive experiments to evaluate the performance of various aspects of the underwater multi-robot platform proposed in this paper.

As shown in Figure 9, the experiments of this section are conducted in a water tank measuring 1.5m×1.2m×0.8m, filled with approximately 50cm of tap water. Additionally, there are some auxiliary devices, including a calibration board, a 14cm diameter red sports ball, and a water scoop that is pressed at the bottom of the water by a stone. Three robots are utilized in the experiments, each connected to a ground computer via cables. The computer serves as the communication medium for the three robots, thereby forming a distributed network. The distributed network in the various experiments of this section adopts a fully connected topology.

The specific implementation of each robot can be referred to in Section 2 of this paper. Various algorithms presented in this paper have certain data that are to be determined, such as the intrinsic matrix of each camera and the transformation matrix from the world coordinate system to the camera coordinate system, all of which are obtained through prior calibration and computation.

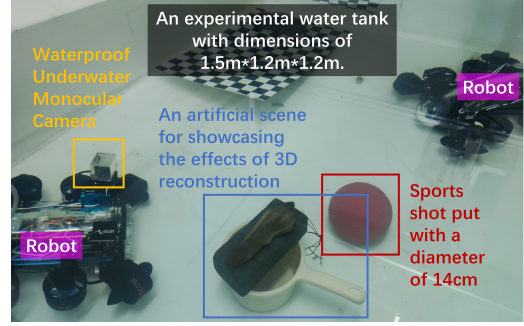


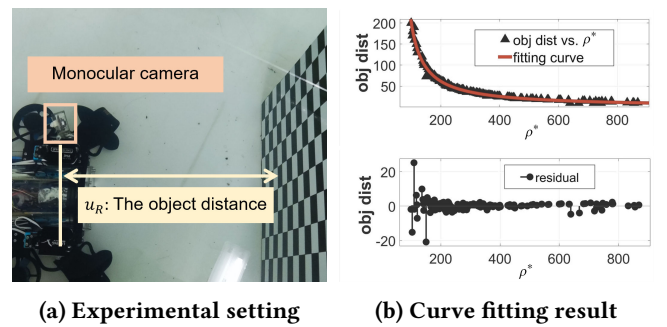
Figure 9: Test bed settings.

### 6.1 Underwater Monocular Depth Imaging

To implement our underwater monocular depth imaging method in practical scenario, the first step is to obtain the function  $h$  in (3). The Figure 10 demonstrates the experimental setup and results of this model calibration process.

As shown in Figure 10a, by altering  $u_R$  the distance between the calibration board and the camera, a series of optimal focal values  $\rho^*$  and corresponding object distances  $u_R$  are obtained. These data are then put into curve fitting toolbox to determine the approximation of  $h$ . According to the fitting results (shown in Figure 10b), we have  $h = \frac{kxf}{kx-f} + c$ , where  $k = 0.3922$ ,  $f = 0.7431$ ,  $c = 0.7577$ . The R-squared of the regression is 0.99, with  $RMSE = 3.4285$ .

The fitting results support our empirical formula proposed in (3), thereby validating the feasibility of our approach to achieve monocular distance measurement based on clarity.



(a) Experimental setting

(b) Curve fitting result

Figure 10: Clarity function calibration experiment.

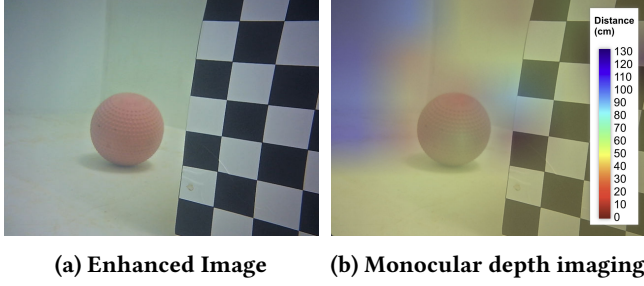


Figure 11: Monocular depth estimation result.

Figure 11 illustrate the depth estimation result using the aforementioned calibrated function. In experiments, the images captured by the camera are enhanced (Figure 11a) in real-time through the LU2Net algorithm [34]. To obtain depth information across the entire field of view, the camera images are partitioned into blocks of 50x50 pixels. The clarity function Tenengrad is computed in each block to determine the optimal focus value in each block. The depths are then calculated and visualized (Figure 11b). It can be observed that this method effectively handles flat surfaces lacking distinctive features, such as the edges and bottom of the tank. Our method distinguishes between them and successfully measures their exact depth.

## 6.2 Distributed Underwater Localization

In this subsection, we choose a sports shot put (lying on the bottom of our experimental tank) as the target object to implement our distributed localization protocol. In the experiment, each robot utilizes the orientation control algorithm proposed in Section 5 of this paper to hover at a depth of approximately 40 cm in the water, using the camera gimbal mounted on the robot to locate the target object at the corresponding position.

As shown in Figure 12a, the world coordinate system is anchored at the lower left corner of the tank's base. In the initial state, robot 1 has the target object within its field of view of camera and is able to obtain the localization estimation of the target object, while robots 2 and 3 do not acquire the position of the object.

The distributed localization results are visualized in Figure 12. In the figure, the numbers within parentheses denote the dimensions. For example,  $\hat{x}_2^t(1)$  represents the first dimension of  $\hat{x}_2^t$ , i.e., the prior estimation of robot 2 at iteration  $t$ . Due to the significant disparity between the first two dimension (XY-coordinates) and the third dimension (Z-coordinates), the visualization is divided into two sets.

It can be observed that at first, only robot 1 has data  $\hat{x}_1^t$ , i.e., the estimated localization of the target object. The positional information of the target object is then continuously conveyed to the other two robots through the iterations of our distributed network. Based on the localization information,

robots 2 and 3 adjust their camera gimbals to search for the target object. They obtain the view of the target object in the 16th and 28th iterations, respectively. After acquiring the view, the robots joined the valid robot set  $S^t$ . Consequently, the distributed protocol we designed also incorporated their measurement information into the network. Ultimately, we achieved a relatively accurate distributed localization with an error margin only at the millimeter level.

Figure 12c and Figure 12d are the prior estimation of the target object, i.e., the localization results without distributed protocol. Figure 12e and Figure 12f are the distributed localization results, which are apparently better than that without distributed protocol, which strongly demonstrate the effectiveness of the algorithm proposed in Section 4.

Figure 12b shows the final state of the experiments. The relative error is **less than 0.4%**. These experiments validate the effectiveness of the distributed localization mechanism of our platform.

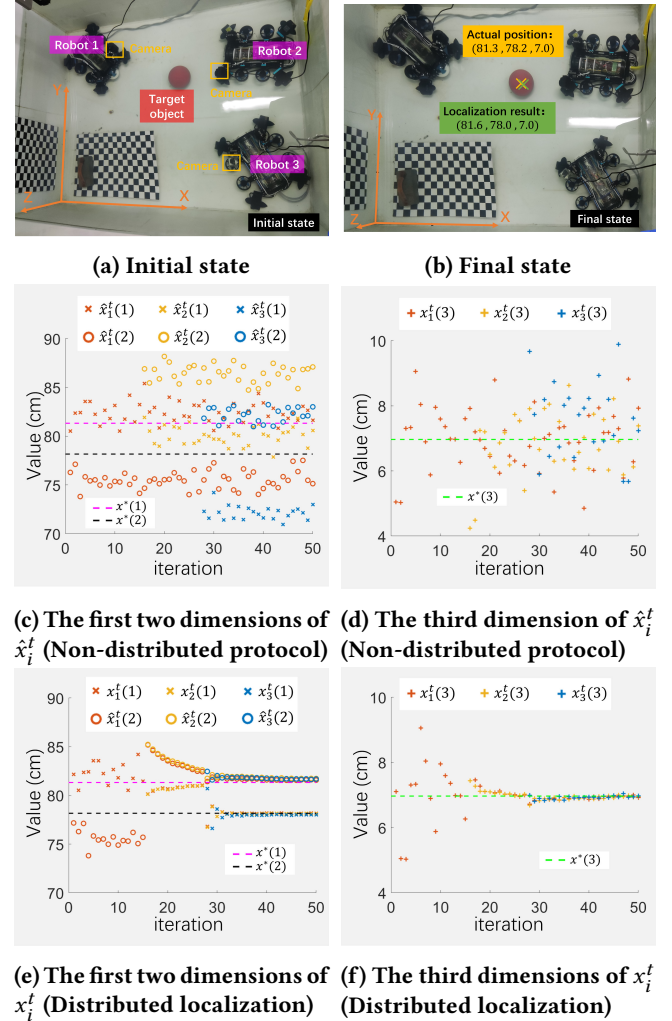


Figure 12: The distributed localization results.

### 6.3 Robust Orientation Control

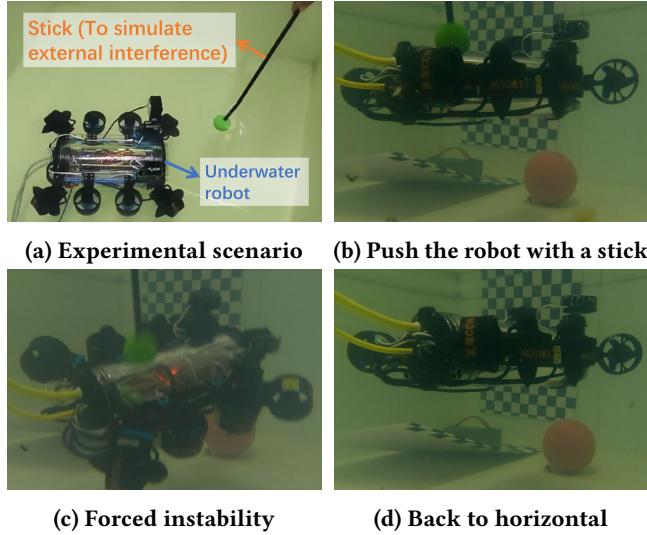


Figure 13: Experiment for robust orientation control.

The experiments in the previous subsection depend on the maintenance of stable posture by each robot throughout the entire process of the localization algorithm. To convincingly demonstrate the robustness of our platform, two experiments are designed in this subsection to verify the disturbance resilience of the orientation control system.

The first experiment is external force disturbance experiment (Figure 13). The robot suspending at the depth of 30cm is pushed by a stick (to simulate external interference). The second experiment is multi-depth suspension experiment, where the robot descends from 22cm to 41cm and maintains horizontal orientation. The data of water pressure sensors and the delta PWM input of the central thrusters are presented in Figure 14.

In the first experiment, despite being forcibly disrupted from a stable state by external disturbances, the system regain its original depth and horizontal orientation in **less than 2 seconds**. The second experiment achieves similar results. These two experiments validate the effectiveness and robustness of our orientation control framework.

### 6.4 Applications

On the foundation of low-cost distributed localization, our platform can also be equipped with additional algorithms to realize a broader range of applications.

**1) Underwater 3D reconstruction.** With the integration of the NeRF algorithm [18], we achieve distributed underwater 3D reconstruction in experimental environment (shown in Figure 9). The results are depicted in Figure 15. Our distributed localization platform make it possible for multiple

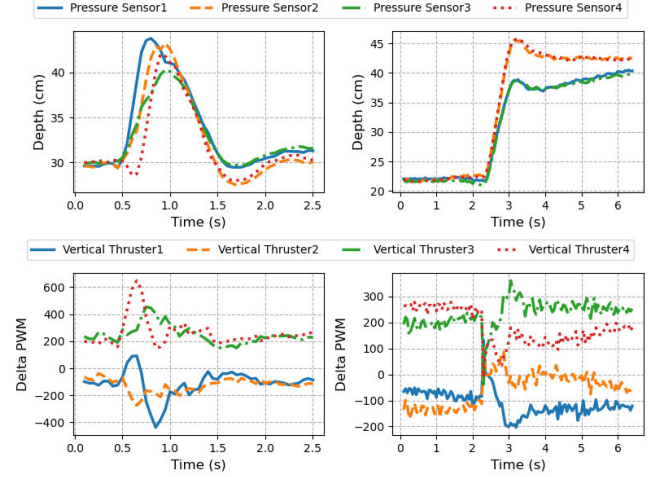


Figure 14: Robust orientation control results.

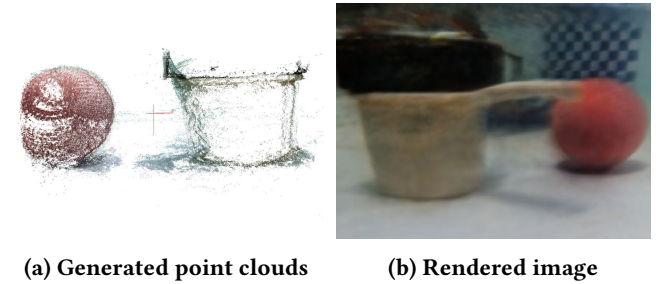


Figure 15: Application: underwater 3D reconstruction.

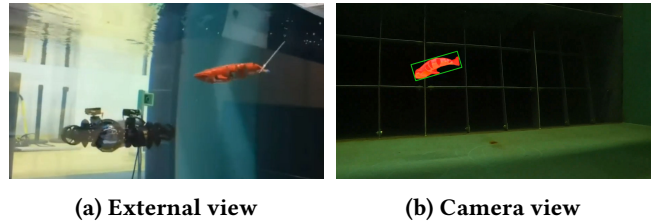


Figure 16: Application: underwater creature tracking.

robots to simultaneously photograph and reconstruct a large-scale underwater scene, with each robot precisely obtaining the location that needs to be reconstructed.

**2) Underwater creature tracking.** As shown Figure 16, by incorporating a target tracking algorithm [33], our platform is also capable of tracking aquatic organisms.

Our multi-robot platform is capable of acquiring the location of the target organism, which aids in achieving more accurate tracking. Moreover, owing to our distributed protocol, as long as one robot in the platform does not lose sight of the underwater target, it can inform the others through the distributed iteration, allowing those that have lost track to reacquire the target organism, significantly enhancing the



robustness of the tracking. This will be of significant importance for tracking organisms that move at extremely high speeds or those in complex, occlusion-rich environments.

## 7 CONCLUSIONS

In this paper, we presented Aucamp, an underwater multi-robot platform that utilize cost-effective monocular cameras to achieve distributed localization. We proposed a Tenengrad-feature-based approach to accomplish depth estimation, coupled with an empirical formula for monocular localization and detailed analysis of its error. Using distributed update protocol, we proposed an effective algorithm to accomplish global localization over the whole multi-robot platform. To support the distributed localization process of our underwater platform, we provided rigorous dynamics model of the multi-thruster robot in our platform and further designed the robust orientation control framework. Extensive experiments and application instances evaluated the effectiveness and robustness of our multi-robot platform.

Future directions include designing a optimal cooperative illumination mechanism based on the imaging system of the proposed platform. The underwater domain, characterized by dimly lit conditions, can be advantageously illuminated by the supplemental lighting fixtures equipped on each robotic unit within our platform. The cooperative illumination capability may greatly improve the viability and usability of camera-based platforms in underwater settings.

## REFERENCES

- [1] Jonas Beuchert and Alex Rogers. 2021. SnapperGPS: algorithms for energy-efficient low-cost location estimation using GNSS signal snapshots. In *Proceedings of the 19th ACM Conference on Embedded Networked Sensor Systems* (Coimbra, Portugal) (SenSys '21). Association for Computing Machinery, New York, NY, USA, 165–177.
- [2] Ling Chen, Sen Wang, Huosheng Hu, Dongbing Gu, and Liqing Liao. 2015. Improving localization accuracy for an underwater robot with a slow-sampling sonar through graph optimization. *IEEE Sensors Journal* 15, 9 (2015), 5024–5035.
- [3] Jack Connor, Benjamin Champion, and Matthew A. Joordens. 2021. Current algorithms, communication methods and designs for underwater swarm robotics: a review. *IEEE Sensors Journal* 21, 1 (2021), 153–169.
- [4] Kevin J DeMarco, Michael E West, and Ayanna M Howard. 2013. Sonar-based detection and tracking of a diver for underwater human-robot interaction scenarios. In *2013 IEEE International Conference on Systems, Man, and Cybernetics*. IEEE, 2378–2383.
- [5] Miguel Duarte, Jorge Gomes, Vasco Costa, Tiago Rodrigues, Fernando Silva, Victor Lobo, Mario Monteiro Marques, Sancho Moura Oliveira, and Anders Lyhne Christensen. 2016. Application of swarm robotics systems to marine environmental monitoring. In *OCEANS 2016 - Shanghai*. 1–8.
- [6] G. Dudek, M. Jenkin, C. Prahacs, A. Hogue, J. Sattar, P. Giguere, A. German, Hui Liu, S. Saunderson, A. Ripsman, S. Simhon, L.-A. Torres, E. Milios, P. Zhang, and I. Rekleitis. 2005. A visually guided swimming robot. In *2005 IEEE/RSJ International Conference on Intelligent Robots and Systems*. 3604–3609.
- [7] Chelsey Edge, Sadman Sakib Enan, Michael Fulton, Jungseok Hong, Jiawei Mo, Kimberly Barthelemy, Hunter Bashaw, Berik Kallevig, Corey Knutson, Kevin Orpen, et al. 2020. Design and experiments with LoCO AUV: A low cost open-source autonomous underwater vehicle. In *2020 IEEE/RSJ International Conference on Intelligent Robots and Systems (IROS)*. IEEE, 1761–1768.
- [8] John Folkesson, John Leonard, Jacques Leederkerken, and Rob Williams. 2007. Feature tracking for underwater navigation using sonar. In *2007 IEEE/RSJ International Conference on Intelligent Robots and Systems*. IEEE, 3678–3684.
- [9] Guanying Huo, Ziyin Wu, Jiabiao Li, and Shoujun Li. 2018. Underwater target detection and 3D reconstruction system based on binocular vision. *Sensors* 18, 10 (2018), 3570.
- [10] Keigo Iizuka and Keigo Iizuka. 2008. *Engineering optics*. Vol. 35. Springer.
- [11] Imad Jawhar, Nader Mohamed, Jameela Al-Jaroodi, and Sheng Zhang. 2019. An architecture for using autonomous underwater vehicles in wireless sensor networks for underwater pipeline monitoring. *IEEE Transactions on Industrial Informatics* 15, 3 (2019), 1329–1340.
- [12] Lai Kang, Lingda Wu, and Yee-Hong Yang. 2012. Experimental study of the influence of refraction on underwater three-dimensional reconstruction using the SVP camera model. *Applied Optics* 51, 31 (Nov 2012), 7591–7603.
- [13] Michael Krieg, Kevin Nelson, and Kamran Mohseni. 2019. Distributed sensing for fluid disturbance compensation and motion control of intelligent robots. *Nature Machine Intelligence* 1 (2019), 216 – 224.
- [14] Pijush K Kundu, Ira M Cohen, and David R Dowling. 2015. *Fluid mechanics*. Academic press.
- [15] Jianfeng Liu, Jiexin Pu, Lifan Sun, and Zishu He. 2019. An approach to robust INS/UWB integrated positioning for autonomous indoor mobile robots. *Sensors* 19, 4 (2019), 950.
- [16] Song Liu and Tian He. 2017. SmartLight: light-weight 3D indoor localization using a single LED lamp. In *Proceedings of the 15th ACM Conference on Embedded Network Sensor Systems* (Delft, Netherlands) (SenSys '17). Association for Computing Machinery, New York, NY, USA, Article 11, 14 pages.
- [17] Martin Ludvigsen and Asgeir J. Sørensen. 2016. Towards integrated autonomous underwater operations for ocean mapping and monitoring. *Annual Reviews in Control* 42 (2016), 145–157.
- [18] Ben Mildenhall, Pratul P Srinivasan, Matthew Tancik, Jonathan T Barron, Ravi Ramamoorthi, and Ren Ng. 2021. Nerf: Representing scenes as neural radiance fields for view synthesis. *Commun. ACM* 65, 1 (2021), 99–106.
- [19] Reza Olfati-Saber and Richard M Murray. 2004. Consensus problems in networks of agents with switching topology and time-delays. *IEEE Trans. Automat. Control* 49, 9 (2004), 1520–1533.
- [20] Chiara Petrioli, Roberto Petrocchia, and Daniele Spaccini. 2013. Adaptive cross-layer routing for underwater acoustic sensor networks with the SUNSET framework. In *Proceedings of the 11th ACM Conference on Embedded Networked Sensor Systems* (Roma, Italy) (SenSys '13). Association for Computing Machinery, New York, NY, USA, Article 80, 2 pages.
- [21] Giacomo Picardi, Mrudul Chellapurath, Saverio Iacoponi, Sergio Steffanni, Cecilia Laschi, and Marcello Calisti. 2020. Bioinspired underwater legged robot for seabed exploration with low environmental disturbance. *Science Robotics* 5, 42 (2020), eaaz1012.
- [22] Fabio Remondino and Clive Fraser. 2006. Digital camera calibration methods: considerations and comparisons. *International Archives of the Photogrammetry, Remote Sensing and Spatial Information Sciences* 36, 5 (2006), 266–272.
- [23] Christian Renner, Benjamin Meyer, Daniel Bimschas, Alexander Gabrecht, Sebastian Ebers, Thomas Tosik, Ammar Amory, Erik Maehle,

- and Stefan Fischer. 2014. Hybrid underwater environmental monitoring. In *Proceedings of the 12th ACM Conference on Embedded Network Sensor Systems (Memphis, Tennessee) (SenSys '14)*. Association for Computing Machinery, New York, NY, USA, 340–341. <https://doi.org/10.1145/2668332.2668354>
- [24] Francisco Rovira-Más, Ishani Chatterjee, and Verónica Sáiz-Rubio. 2015. The role of GNSS in the navigation strategies of cost-effective agricultural robots. *Computers and Electronics in Agriculture* 112 (2015), 172–183.
- [25] Wang Shule, Carmen Martínez Almansa, Jorge Peña Queralta, Zhuo Zou, and Tomi Westerlund. 2020. UWB-based localization for multi-UAV systems and collaborative heterogeneous multi-robot systems. *Procedia Computer Science* 175 (2020), 357–364.
- [26] N. Vedachalam, R. Ramesh, V. Bala Naga Jyothi, V. Doss Prakash, and G. A. Ramadass. 2019. Autonomous underwater vehicles - challenging developments and technological maturity towards strategic swarm robotics systems. *Marine Georesources & Geotechnology* 37, 5 (2019), 525–538.
- [27] Jie Wang, Qinghua Gao, Yan Yu, Xiao Zhang, and Xueyan Feng. 2015. Time and energy efficient TOF-based device-free wireless localization. *IEEE Transactions on Industrial Informatics* 12, 1 (2015), 158–168.
- [28] Shijun Wang, Aixue Ye, Hao Guo, Jiaojiao Gu, Xiaonan Wang, and Kui Yuan. 2016. Autonomous pallet localization and picking for industrial forklifts based on the line structured light. In *2016 IEEE International Conference on Mechatronics and Automation*. IEEE, 707–713.
- [29] Christopher JCH Watkins and Peter Dayan. 1992. Q-learning. *Machine Learning* 8 (1992), 279–292.
- [30] Gary Witus and Shawn Hunt. 2008. Monocular visual ranging. In *Unmanned Systems Technology X*, Vol. 6962. SPIE, 38–44.
- [31] Ryan W Wolcott and Ryan M Eustice. 2015. Fast LIDAR localization using multiresolution Gaussian mixture maps. In *2015 IEEE International Conference on Robotics and Automation (ICRA)*. IEEE, 2814–2821.
- [32] Xiaojun Wu and XingCan Tang. 2019. Accurate binocular stereo underwater measurement method. *International Journal of Advanced Robotic Systems* 16, 5 (2019), 1729881419864468.
- [33] Bin Yan, Houwen Peng, Kan Wu, Dong Wang, Jianlong Fu, and Huchuan Lu. 2021. LightTrack: Finding lightweight neural networks for object tracking via one-shot architecture search. In *Proceedings of the IEEE/CVF Conference on Computer Vision and Pattern Recognition*. 15180–15189.
- [34] Haodong Yang, Jisheng Xu, Zhiliang Lin, and Jianping He. 2024. LU2Net: a lightweight network for real-time underwater image enhancement. *arXiv e-prints* (Jun 2024), arXiv:2406.14973.